A Unified Open-Circuit-Voltage Model of Lithium-ion Batteries for State-of-Charge Estimation and State-of-Health Monitoring ☆

Caihao Weng[a,*], Jing Sun[a], Huei Peng[b]

[a] *Department of Naval Architecture and Marine Engineering, University of Michigan, Ann Arbor, Michigan, 48109, USA*
[b] *Department of Mechanical Engineering, University of Michigan, Ann Arbor, Michigan, 48109, USA*

Abstract

Open-Circuit-Voltage (OCV) data is widely used for characterizing battery properties under different conditions. It contains important information that can help to identify battery state-of-charge (SOC) and state-of-health (SOH). While various OCV models have been developed for battery SOC estimation, few have been designed for SOH monitoring. In this paper, we propose a unified OCV model that can be applied for both SOC estimation and SOH monitoring. Improvements in SOC estimation using the new model compared to other existing models are demonstrated. Moreover, it is shown that the proposed OCV model can be used to perform battery SOH monitoring as it effectively captures aging information based on incremental capacity analysis (ICA). Parametric analysis and model complexity reduction are also addressed. Experimental data is used to illustrate the effectiveness of the model and its simplified version in the application context of SOC estimation and SOH monitoring.

Keywords: Electric vehicles, Lithium-ion batteries, Open-Circuit-Voltage, State-of-Charge, State-of-Health, Incremental capacity analysis

1. Introduction

The growing concern over oil shortage and environmental issues has greatly accelerated the development of alternative power and energy solutions to displace fossil fuel in recent years [1–3]. As an important component in the clean energy intuitive, energy storage system is a critical enabler for the next generation power/energy technologies. Among the various choices of energy storage technologies, it is well recognized that battery systems can offer a number of high-value opportunities given their advantages in portability and energy efficiency, particularly for mobile applications [4]. Given the fact that batteries have been used to power an increasingly diverse range of applications, from cell phones to electric vehicles, more reliable and efficient battery management systems (BMSs) need to be developed [5].

BMS has, among many functions, two important tasks, namely the state-of-charge (SOC) estimation and state-of-health (SOH) determination [6, 7]. SOC is commonly defined as "the percentage of the maximum possible charge that is present inside a rechargeable battery", and the estimation of SOC serves as the fuel gauge for batteries. On the other hand, SOH is "a 'measure' that reflects the general condition of a battery and its ability to deliver the specified performance in comparison with a fresh battery" [8]. Typically, the quantitative definition of SOH is based either on the battery capacity or the internal resistance, depending on specific applications [7]. Due to the requirement for online estimation of both SOC and SOH during system operation, the development of an simple but accurate battery model is crucial for an effective and robust BMS.

Many studies of battery SOC estimation have been reported in the literature (see Ref. [9] and references therein). Most of those methods are model-based approach and require an accurate open-circuit-voltage (OCV) model which relates OCV to SOC [9–11]. The OCV-SOC function is implemented in the BMS either as a look-up table or an analytical expression, while the latter has several advantages including computational efficiency (since no interpolation is needed) as well as

☆This work is supported by US-China Clean Energy Research Center-Clean Vehicle Consortium (CERC-CVC).

*Corresponding author. Tel.:+1 734 763 7963; fax:+1 734 936 8820

Email addresses: chsweng@umich.edu (Caihao Weng), jingsun@umich.edu (Jing Sun), hpeng@umich.edu (Huei Peng)

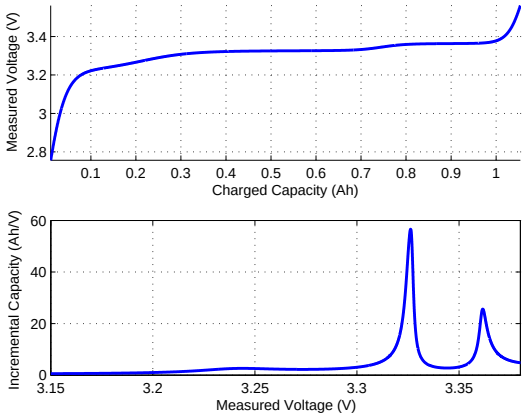

Figure 1: ICA performed on charging voltage curve at $\frac{1}{20}$ C rate

the convenience for analysis. Because of the wide flat region on the OCV-SOC curve for lithium iron phosphate batteries, a small mismatch in OCV fitting may cause a large deviation in SOC estimation. Therefore, improving OCV models can contribute significantly to increasing the accuracy of SOC estimation.

In Ref. [12], several phenomenological OCV models, which are built with curve fitting without considering the complex battery physical behavior during the lithium-ion intercalaction/deintercalation process [1, 13], are summarized. Although those models represent part of the nonlinear characteristics of battery OCV, they fail to capture the voltage plateaus and transitions (please see Fig. 1) that correspond to the staging phenomenon at the graphite anode [7, 14–17].

The modeling of OCV-SOC function is also found to be crucial when it comes to battery SOH monitoring, as OCV data often reflect battery aging and performance degradation [18]. In particular, by differentiating the battery charged capacity (Q) with respect to the terminal voltage (V), the voltage plateaus on the OCV curve is transformed into clearly identifiable dQ/dV peaks on the incremental capacity (IC) curve (see Fig. 1) [7, 14, 19]. This so-called incremental capacity analysis (ICA) technique helps to detect gradual changes in cell behavior, based on OCV data collected from life cycle test, with greater sensitivity than those based on conventional methods [5].

One major difficulty in performing ICA analysis is its sensitivity to noise in battery voltage measurement. Since all the peaks on an IC curve lie within the flat region of the OCV curve, computing the derivatives directly from the data could lead to inaccurate and undesirable results, even after careful data filtering [7]. By constructing an OCV model that represents the underlying physical phenomenon of lithium-ion intercalaction/deintercalation process and therefore captures the subtle transitions over the flat region, one can take advantage of the analytical form of the model to extract useful information associated with battery electrochemical properties and aging status using ICA [5, 20]. Therefore, for both SOC estimation and SOH monitoring through ICA, an OCV model that can capture the physical process over the flat region of the OCV-SOC curve and be capable of supporting ICA is needed.

In this paper, we propose a unified OCV-SOC model that is intended for both SOC estimation and SOH monitoring. The study is based on a battery life cycle test data set collected from eight A123 $LiFePO_4$ cells over a period of 18 months [7, 21].

The remainder of this paper is organized as follows. We first propose the development and parametrization of the new OCV model in Section 2. Then we compare the new OCV model with other existing models in terms of OCV data fitting and SOC estimation accuracy in Section 3. In Section 4, we elucidate the application of the OCV model for SOH monitoring, followed by parametric analysis and model simplification in Section 6. The conclusions are given in Section 7.

2. A New Open-Circuit-Voltage Model

We propose a new OCV model structure that can capture the phenomenological characteristics associated with the lithium-ion intercalaction/deintercalation process while fitting the OCV-SOC data. A specific model structure is chosen to enforce the model to exhibit plateaus on the OCV curve. These plateaus are results from the lithium-ion staging phenomena, and have been irrefutably observed from experimental data. The parameters of the proposed model will be identified with experiment data. Instead of measuring the OCV after a long relaxation period at different SOC levels that span the entire range, the data used are collected by charging/discharging a $LiFePO_4$ battery cell at low rate of $\frac{1}{20}$ C. The voltage data obtained by this slow charging/discharging process reflects the OCV at a close-to-equilibrium status [19]. Although the close-to-equilibrium OCV curve shown in Fig. 2 may be affected by hysteresis and diffusion voltage due to lack of relaxation, it can sufficiently represent the generic electrochemical properties for ICA and quantifying capacity fading as presented in Ref. [19]. The upper and lower cut-off voltage limits are set to be 3.6 V and 2.1 V respectively. The total charge stored between the upper and lower limits is defined as the battery total capacity.

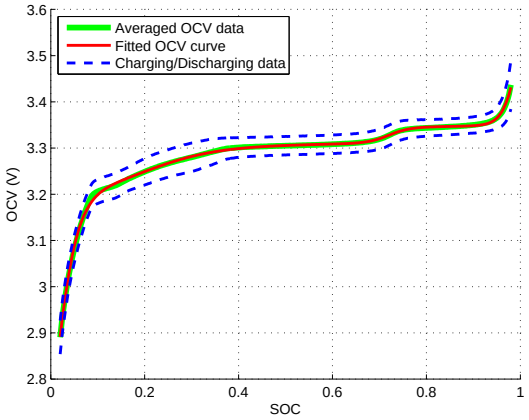

Figure 2: Fitting result with the proposed OCV model

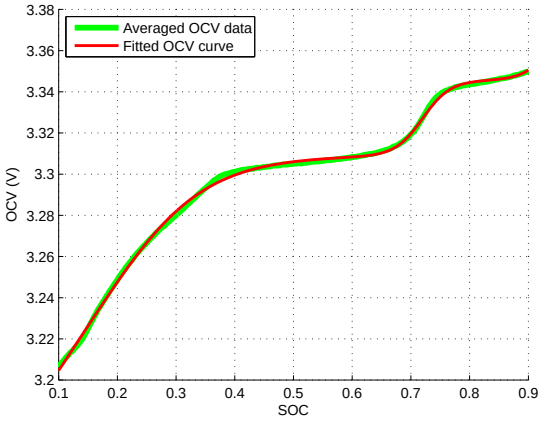

Figure 3: OCV model fitted over SOC from 10% to 90%

2.1. Open-Circuit-Voltage Parametric Model

Based on the studies presented in Refs. [7, 14, 19], there are generally three observable voltage plateaus and two transitions, which are important in characterizing the OCV and battery capacity, over the flat area on the OCV curve of $LiFePO_4$ battery cells. In our model, those plateaus and transitions are represented by the sigmoid functions as follows,

$$\begin{aligned} OCV(z) =& K_0 + K_1 \frac{1}{1+e^{\alpha_1(z-\beta_1)}} + K_2 \frac{1}{1+e^{\alpha_2(z-\beta_2)}} \\ &+ K_3 \frac{1}{1+e^{\alpha_3(z-1)}} + K_4 \frac{1}{1+e^{\alpha_4 z}} + K_5 z \end{aligned} \quad (1)$$

where z is the SOC, $K_{0\sim5}$ are the linear parameters, and $\alpha_{1\sim4}$ and $\beta_{1\sim2}$ are the nonlinear parameters. This parametrization shares features with some of the electrochemical model of $LiFePO_4$ proposed in Ref. [1]. More specifically, our model can be interpreted as a simplified composition and generalization of the cathode and anode OCV functions in Ref. [1] (where hyperbolic and exponential functions are used).

An example of a complete data set for model identification is shown in Fig. 2, where the collected charging/discharging data are averaged to yield OCV data. The parameters in Eq. (1) are determined using the Matlab curve fitting toolbox. We focus on fitting the data in the middle SOC range, namely 10%-90% SOC, given that in practice only data in the middle SOC range are available. Moreover, this allows us to achieve higher accuracy in the range where the model will be most useful. The fitted OCV-SOC curve is plotted in Fig. 3, with a reference made to the averaged measured OCV data. The rms and maximum values of fitting error is 1 mV and 2.5 mV, reduced from 2.3 mV (rms)and 7 mV (maximum) that were obtained when the full SOC range is used.

Table 1: OCV models summarized in Ref. [12] together with the new model

#		OCV Models	Ref.
1	$OCV(z) =$	$K_0 - \frac{K_1}{z} - K_2 z + K_3 \ln(z) + K_4 \ln(1-z)$	[22]
2	$OCV(z) =$	$K_0 + K_1(1-e^{-\alpha_1 z}) + K_2(1-e^{-\frac{\alpha_2}{1-z}}) + K_3 z$	[23]
3	$OCV(z) =$	$K_0 + K_1 e^{-\alpha_1(1-z)} - \frac{K_2}{z}$	[24]
4	$OCV(z) =$	$K_0 + K_1 e^{-\alpha_1 z} + K_2 z + K_3 z^2 + K_4 z^3$	[25]
5	$OCV(z) =$	$K_0 + K_1 z + K_2 z^2 + K_3 z^3 + K_4 z^4 + K_5 z^5 + K_6 z^6$	[26]
6	$OCV(z) =$	$K_0 + K_1 \frac{1}{1+e^{\alpha_1(z-\beta_1)}} + K_2 \frac{1}{1+e^{\alpha_2(z-\beta_2)}}$	Proposed
		$+K_3 \frac{1}{1+e^{\alpha_3(z-1)}} + K_4 \frac{1}{1+e^{\alpha_4 z}} + K_5 z$	Model

2.2. Model Comparison and Analysis

The new OCV model is compared in this section with the five different models summarized in Ref. [12], where the polynomial model is reported to be the most accurate. All the parameters in those five OCV models are refitted for the data presented in Fig. 2 using Matlab curve fitting toolbox, the results with their rms and maximum errors are shown and summarized in Fig. 4 and Tab. 2. It should be noted that none of the five OCV models is suitable for IC analysis, as their model structures do not take into account the staging mechanism in intercalation/deintercalation process. One can see that the new OCV model proposed in Eq. 1 has better fitting accuracy than all those five models. Consequently, improvement in the SOC estimation results may also be expected when the new OCV model is incorporated.

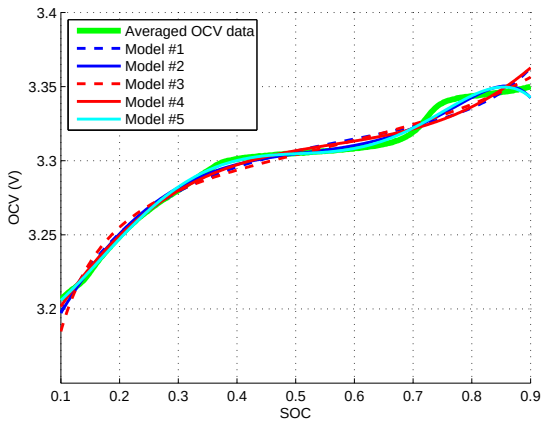

Figure 4: Comparison of OCV fitting results

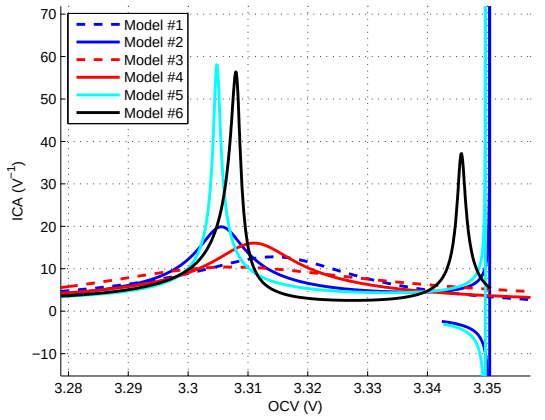

Figure 5: Comparison of IC curves from fitted OCV

The IC curves based on different OCV models are shown in Fig. 5. It can be observed that the new model (model #6) captures the two IC peaks associated with staging, whereas all other models only show one peak on the IC curves. Therefore, model #6 can extract more capacity information from the OCV data compared to other models and will be used for further analysis in SOH monitoring. For models #2 and #5, dQ/dV is not defined at 3.35 volt because of a singularity in the math expression. Consequently, spikes in both directions are shown in Figure 5 for the two IC curves, corresponding to models #2 and #5.

Table 2: Fitting results of OCV models from Tab. 1

Model #	RMS Error (mV)	Max Error (mV)
1	5.2	12.6
2	3.1	8.9
3	5.6	21.3
4	4.7	12.7
5	2.1	7.3
6	1.0	2.5

3. State-of-Charge Estimation Based on Extended Kalman Filter

The extended Kalman filter (EKF) based approach discussed in Ref. [27] is used to illustrate the implementation of the new OCV model for SOC estimation. The battery test data for this study is collected through the experimental set-up introduced in Ref. [21] and the first-order RC model [28] is used for calculating the SOC with the following algorithm:

RC Model:

$$z_{k+1} = f(z_k, I_k) + w_k,$$
$$V_k = g(z_k, I_k) + v_k,$$

EKF Algorithm:

$$A_{k-1} = \left.\frac{\partial f(z_{k-1}, I_{k-1})}{\partial z_{k-1}}\right|_{z_{k-1}=\hat{z}_{k-1}},$$
$$C_k = \left.\frac{\partial g(z_k, I_k)}{\partial z_k}\right|_{z_k=\hat{z}_{k|k-1}},$$
$$\hat{z}_{k|k-1} = f(\hat{z}_{k-1}, I_{k-1}),$$
$$P_{k|k-1} = A_{k-1}P_{k-1}A_{k-1}^T + Q,$$
$$G_k = P_{k|k-1}C_k^T\left[C_kP_{k|k-1}C_k^T + V\right]^{-1},$$
$$\hat{z}_k = \hat{z}_{k|k-1} + G_k\left[V_k - g(\hat{z}_{k|k-1}, I_k)\right],$$
$$P_k = \left[\mathbf{I} - G_kC_k\right]P_{k|k-1},$$

where

$$f(z_k, I_k) = z_k - (\frac{\eta_i\Delta t}{Q_c})I_k,$$
$$g(z_k, I_k) = OCV(z_k) + V_{rc,k} + R_0I_k,$$
$$V_{rc,k+1} = \exp(\frac{-\Delta t}{R_1C})V_{rc,k} + R_1[1 - \exp(\frac{-\Delta t}{R_1C})]I_k, \quad (2)$$

z_k is the SOC, η_i is the charging/discharing efficiency, Δt is the time step, Q_c is the battery capacity, I_k is the input current, V_k is the total terminal voltage, $V_{rc,k}$ is voltage of the RC circuit, R_0, R_1 and C are battery internal resistance and capacitance, Q is the error covariance

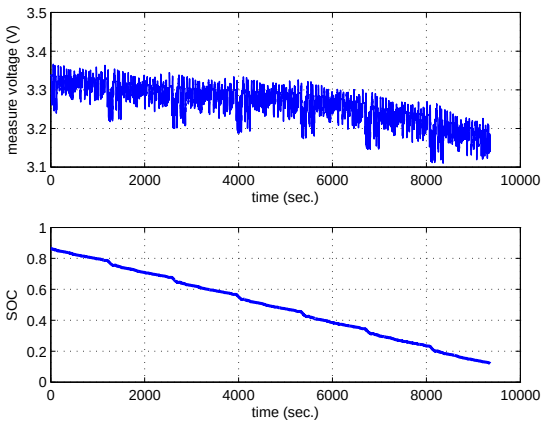

Figure 6: Battery data tested under FUDS

of process noises, and V is the error covariance of observation noises [21]. The OCV function is represented by the model given by Eq. (1).

In this study, all the parameters in the RC model are set to be constants without performing iterative optimizations as discussed in Ref. [12].

The battery data tested under the Federal Urban Driving Schedule (FUDS) is shown in 6. As in Ref. [27], the SOC data obtained by Coulomb counting in the Arbin battery test bench, where high precision current sensor is used, is assumed to be the "true" SOC and used as a reference for performance evaluation. Therefore the SOC estimation error is defined as,

$$e_{SOC,k} = \hat{z}_k - z_k \tag{3}$$

where $e_{SOC,k}$ is the SOC estimation error, $\hat{z}_k$ is the SOC estimated by the EKF algorithm and z_k is the reference SOC calculated from the measured data. Please note that the SOC from Arbin Coulomb counting, while representing the best reference that we can get, is only approximately accurate due to the unavoidable error and integral accumulation of the error in the current measurement [27].

The model parameters used in the EKF based SOC estimation are shown in Tab. 3.

A detailed description of the EKF algorithm can be found in both Refs. [27] and [12]. The parameters of the EKF (i.e., V and Q used in Eq. 2) are calibrated using the data collected in our aging tests, and the same parameters (listed in Tab. 4) are used in the performance evaluation for the new model (#6) and the polynomial model (#5).

Figure 7 displays the EKF based SOC estimation results. The two plots represent two cases with different

Table 3: Parameters of models #5 and #6 used in SOC estimation

Model Parameters	Model #5	Model #6
K_0	3.0896	3.4002
K_1	1.1627	0.0080
K_2	-2.3821	0.0785
K_3	2.1870	-0.2150
K_4	-0.5444	-1.3032
K_5	-0.1939	0.0891
K_6	0.0582	N/A
α_1	N/A	-14
α_2	N/A	-18
α_3	N/A	28
α_4	N/A	40

Table 4: Parameters of EKF based SOC estimator

Parameters	Values
Error covariance of process noises, Q	$\begin{pmatrix} 0.15 & 0 \\ 0 & 1 \end{pmatrix}$
Error covariance of observation noises, V	0.01

initial SOC error (+10% and -10% respectively). One can see that the estimated SOC converge into the 5% estimation error bound when either model #5 or #6 is used. In particular, with positive initial error, the SOC estimated with model #6 converges much faster than the SOC estimated with model #5. This difference in convergence rate with positive initial error can be explained by the curve fitting results shown in Figs. 3 and 4, where model #6 have better accuracy than #5 in the high SOC region. On the other hand, both models have approximately the same accuracy when SOC is below 70% and therefore have similar convergence rate with negative initial error. The 5% error bound can be achieved with other initial error (e.g., 20% or 30%).

In summary, the new OCV model performs well in EKF based SOC estimation. The model delivers accurate estimation results with less than 5% errors without extensive calibration and training. The results presented in this section demonstrates the potential of implementing this new OCV model for SOC estimation problems.

4. State-of-Health Monitoring Based on Incremental Capacity Analysis

Even though ICA was originally proposed for "close-to-equilibrium" conditions, it was shown in Ref. [7]

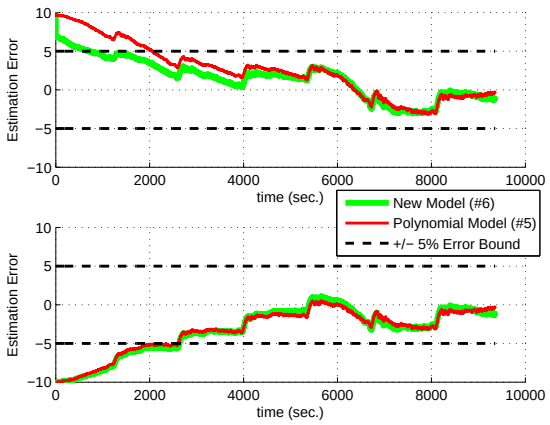

Figure 7: SOC estimation with OCV model #6

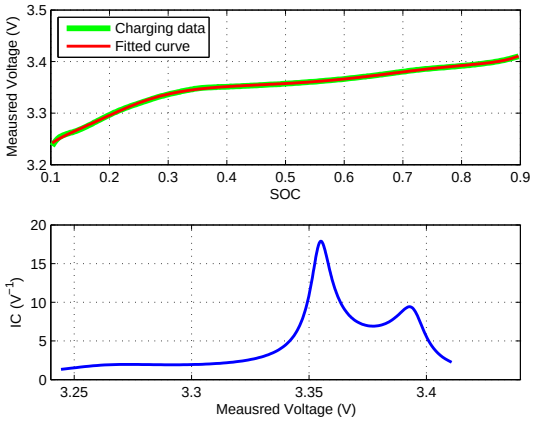

Figure 8: V-SOC and IC curve from 0.5C charging data

that, for normal charging data, the peaks on the IC curve can also be identified and they reveal significant information about battery SOH. Hence, the results presented in this section for ICA are all based on 0.5C battery charging data (same as in Ref. [7]). It will be shown that the proposed parametrization is applicable to both OCV data and normal charging data (i.e., charged at 0.5C).

As shown in Fig. 8, where the charging data is fitted with the model given by Eq. (1) with OCV replaced by the terminal voltage collected at normal charging rate, we can obtain the IC curve directly by differentiating the analytical V-SOC function and then taking the reciprocal.

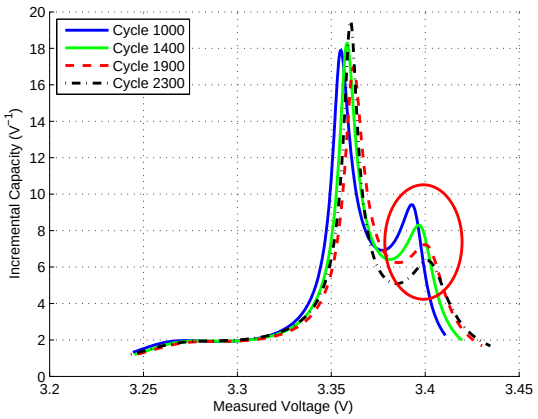

Figure 9: IC curves of data at different aging stages

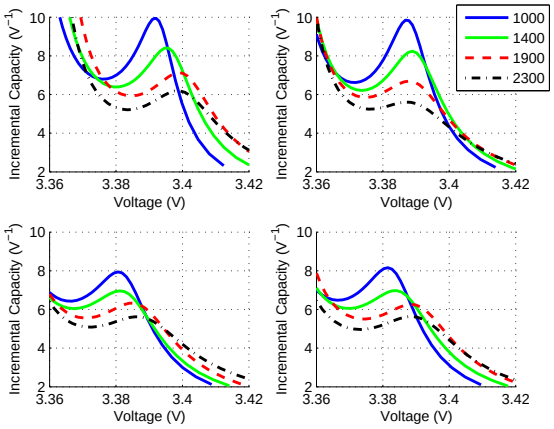

Figure 10: IC curves comparison from four different cells

4.1. Incremental Capacity Analysis at Different Aging Stages

The IC curves of battery charging data collected at different aging cycles under 35^oC environment condition are shown in Fig. 9. The numerical values in the plot legends represent the aging cycle number. The IC peaks highlighted by the circle in Fig. 9 clearly shows a monotonic decreasing trend as battery ages, which implies a battery degradation that is mainly related to the loss of active material at the graphite anode [14, 19].

The IC curves from four different cells are plotted in Fig. 10, where the plots focus on the second peak on the IC curve and depict a consistent trend in capacity fading as reflected by the decreasing IC peaks.

To obtain the correlation between the cell capacity fading and IC peak, the peak values of eight cells at different aging stages are identified. The normalized peak

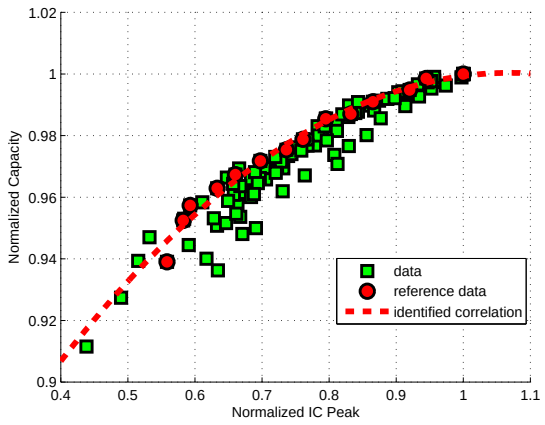

Figure 11: Correlation between faded battery capacity and IC peak values

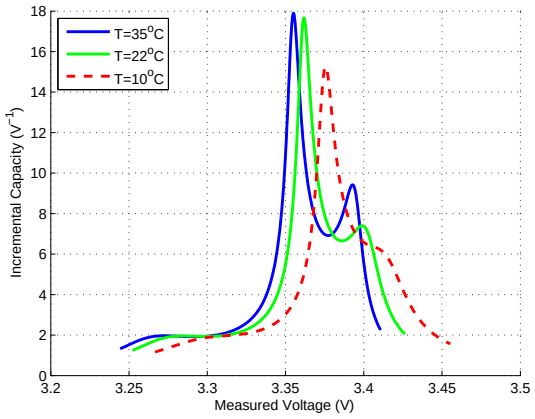

Figure 12: IC curves of data at different temperature

values of one of the cells (red dots in Fig. 11) is correlated with the faded cell capacities, and used to construct the battery capacity estimation curve (red dashed curve in Fig. 11) as done in Ref. [7]. The data from other cells are also plotted to verify the prediction capability of the estimation curve. The result shows the new parametric model in the form of Eq. (1) can be used for capacity based battery SOH monitoring with good accuracy.

4.2. Incremental Capacity Analysis at Different Temperature

Test data were also collected at different temperature throughout the battery aging process. ICA was performed with respect to different temperatures to evaluate and confirm the sensitivity to temperature and results

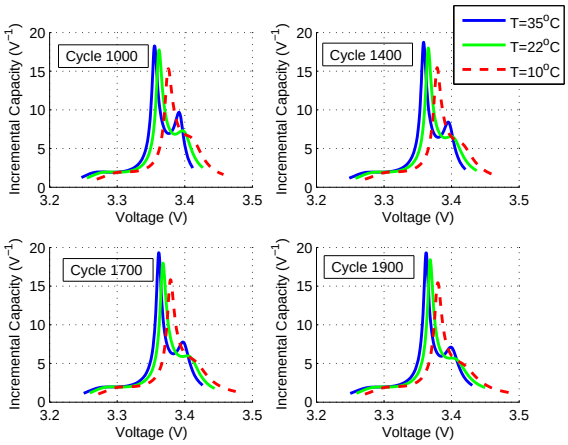

Figure 13: IC curves of data at different temperature and ages

are presented in Fig. 12. The intensities of the IC peaks reduce as temperature drops, which could be attributed to the slow lithium-ion diffusion or lithium plating phenomenon at low temperature as elucidated in Ref. [29]. When the temperature is too low, say at 10^oC, the second peak could disappear from the IC curve. However, since the operating temperature of battery systems are usually maintained through integrated thermal control in the BMS, the disappearance of IC peaks at low temperature should not be a concern.

Figure 13 presents the IC curves at different temperature at different aging stages. A temperature dependence of the IC peaks and the model parameters may be evaluated. The first peak on these four plots shows consistent temperature sensitivity while the second peak shows the aging status. It suggests that the test data corresponding to higher temperature will be more reliable for ICA and capacity fading identification.

5. Other Signatures on the IC Curve and Their Correlation with Capacity Fading

Other than using the IC peak value decreasing as the indication of battery capacity fading, we also explore a different approach that uses the IC peak locations to evaluate the degradation. Since the IC peaks represent the phase transitions during the intercalaction/deintercalation process and this electrochemical reaction is affected by battery capacity loss, the locations of the peaks might also have a correlation with the faded capacity and can give a good estimation of the loss.

Consider the IC as a function of SOC (rather than measured voltage), as shown in Fig. 14. Note that the first IC peak stays at approximately the same location

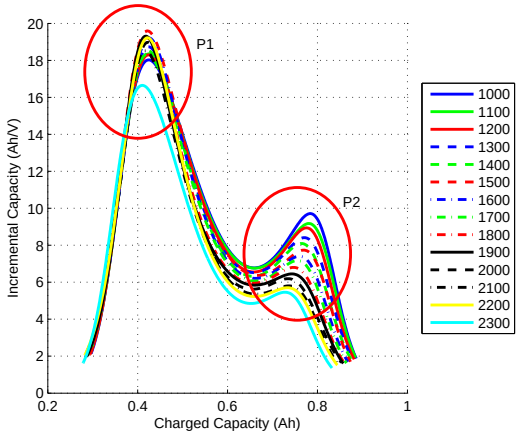

Figure 14: IC curve plotted versus charged capacity data

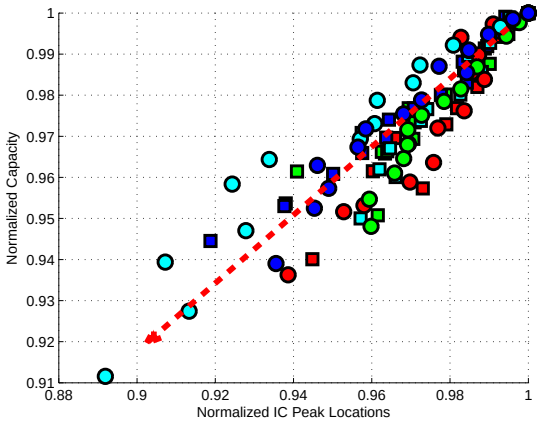

Figure 15: Correlation between IC peak locations and battery faded capacities

whereas the second peak is moving towards the left as the battery ages and capacity decreases. By normalizing both the second IC peak location and battery capacity, we obtain the correlation between the two values in Fig. 15 (data from different cells are color coded differently), which confirms that the location of the second IC peak could also be a indication of battery capacity fading.

However, in order to accurately measure this peak location in terms of charged capacity, it is required to start the battery charging from zero SOC, which is not always practical in real operation. This problem can be addressed by using the SOC span between the two consecutive IC peaks,

$$d_{IC} = P_2 - P_1 \tag{4}$$

where d_{IC} is the SOC interval between two consecutive

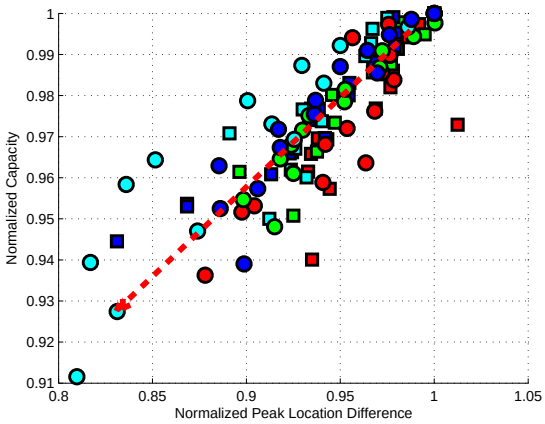

Figure 16: Correlation between IC peak location difference and battery faded capacities

peaks, P_1 and P_2 are the locations of the two IC peaks respectively. The value of d_{IC} is more easily obtainable as long as the charging starts below the SOC value that corresponds to the first IC peak. Typically, the first peak on the IC curve appears around SOC=0.45. Therefore, for all the data we have, this condition is satisfied as long as the charging covers 40% to 85% SOC. The plot with normalized d_{IC} and battery capacity is shown in Fig. 16. This correlation obtained using d_{IC} is looser than using P_2 only, as the values of both P_1 and P_2 are affected by measurement noises and the value of d_{IC} is more susceptible to noise and modeling error.

The analysis suggests that the signatures on the IC curves, namely the second IC peak and the distance between two peaks, can be used as indicators for battery aging. The two correlations based on IC peak locations are not as strong and robust compared to the results based on peak values shown in Fig. 11. Nevertheless, we believe that those correlations can provide useful information for battery SOH monitoring from different perspectives. It is also possible to improve the peak location based results when more accurate current sensors are available.

6. Parametric Analysis and Model Simplification

Although the identification results using the new OCV model has shown its effectiveness, the high number of parameters and nonlinearity of the model may present a challenge for on-board implementation. A parametric analysis is performed to characterize the correlations between model parameters and battery aging, evaluate the sensitivity and robustness of the model

structure, and better understand the utility of the proposed model. Moreover, the analysis results may help to identify the significance of each parameter and simplify the model, so that the computational efficiency in estimation can be improved.

Consider the following function, which is derived by differentiating OCV with respect to the battery SOC,

$$\begin{aligned} G(z) =& \frac{d}{dz} OCV(z) = -K_1 \frac{\alpha_1 e^{\alpha_1(z-\beta_1)}}{(1+e^{\alpha_1(z-\beta_1)})^2} \\ & - K_2 \frac{\alpha_2 e^{\alpha_2(z-\beta_2)}}{(1+e^{\alpha_2(z-\beta_2)})^2} - K_3 \frac{\alpha_3 e^{\alpha_3(z-\beta_3)}}{(1+e^{\alpha_3(z-1)})^2} \\ & - K_4 \frac{\alpha_4 e^{\alpha_4(z-\beta_4)}}{(1+e^{\alpha_4 z})^2} + K_5. \end{aligned} \tag{5}$$

Note that the IC curve is the inverse of $G(z)$, the locations and values of IC peaks may be calculated by letting the derivative of $G(z)$ equal to zero and solving the resulting algebraic equation. The resulting equation, however, is highly nonlinear and cannot be easily solved analytically in general. Here, an alternative approach that separates and analyzes the terms in the Eq. (5) individually is used to correlate the model parameters and the solution of $G(z)$.

To understand the contribution of each term of (5), we first define the following,

$$\begin{aligned} f_1(z) =& -K_1 \frac{\alpha_1 e^{\alpha_1(z-\beta_1)}}{(1+e^{\alpha_1(z-\beta_1)})^2}, \\ f_2(z) =& -K_2 \frac{\alpha_2 e^{\alpha_2(z-\beta_2)}}{(1+e^{\alpha_2(z-\beta_2)})^2}, \\ f_3(z) =& -K_3 \frac{\alpha_3 e^{\alpha_3(z-1)}}{(1+e^{\alpha_3(z-1)})^2}, \\ f_4(z) =& -K_4 \frac{\alpha_4 e^{\alpha_4(z)}}{(1+e^{\alpha_4 z})^2}. \end{aligned} \tag{6}$$

Through analytical and numerical analysis, we have the following observations:

- f_2 and f_4 decay to zero at the high SOC range, where the IC peak of interest occurs. Therefore, they do not contribute to the IC peaks and their locations. Our analysis will be focused on f_1 and f_3;
- The parameter K_5 is a constant and therefore it does not need to be considered here;
- Numerical results show that K_1 and K_3 do not vary much compared to α_1 and α_3;
- Our analysis show that the IC peak has about equal sensitivity to α_1 and α_3. The sensitivity analysis is performed by numerically evaluating the partial derivative of the IC function, defined by $\frac{1}{G(z)}$ with $G(z)$ given by (5), with respect to the parameters α_1 and α_3 at the z value where the second IC peak is located.

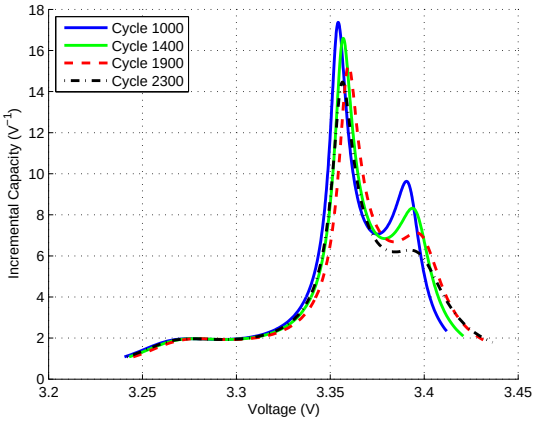

Figure 17: IC curves obtained using simplified OCV model

Table 5: Comparison of fitting accuracy between full and simplified model using RMS error

Cycle #	Full Model (mV)	Reduced-Order Model (mV)
1000	0.760	0.805
1400	0.925	0.980
1900	0.946	1.247
2300	1.024	1.559

With the above observations, we identified a simplified model in the following form:

$$\begin{aligned} OCV(z) =& K_1 \frac{1}{1+e^{\alpha_1(z-\bar{\beta}_1)}} + K_3 \frac{1}{1+e^{\alpha_3(z-1)}} \\ & + \bar{K}_0 + \bar{K}_2 \frac{1}{1+e^{\bar{\alpha}_2(z-\bar{\beta}_2)}} + \bar{K}_4 \frac{1}{1+e^{\bar{\alpha}_4 z}} + \bar{K}_5 z. \end{aligned} \tag{7}$$

where the model structure contains only 4 changing parameters (i.e., K_1, K_3, α_1 and α_3), and other parameters are kept constants as batteries age.

In Fig. 17, one can see that the IC curves obtained using the simplified OCV model show qualitatively the same trend as the ones obtained by the full model (see Fig. 9) when the battery ages. Table 5 shows the comparison of fitting accuracy between the full and the simplified model. In the worst case, the rms error is less than 2 mV. Therefore, the simplification preserves the high fitting accuracy provided by the full model.

Table 6: Parameters of the simplified OCV model

Cycle #	α_1	K_1	α_3	K_3
1000	-12.57	0.0446	25.9352	-0.2459
1400	-12.29	0.0467	23.2749	-0.2435
1900	-11.57	0.0497	20.4778	-0.2413
2300	-11.4	0.0531	18.5991	-0.2447

The parameters for the simplified model are listed in Tab. 6, where one can see the variations in α_1 and α_3 agree with our parametric analysis. Moreover, it suggests that the values of the deteriorating peaks in the IC curves might be estimated directly from the parameters with the following relationship,

$$q = \theta_0 + \theta_1\alpha_1 + \theta_2 K_1 + \theta_3\alpha_3, \tag{8}$$

where q, defined as $q = \frac{p-p_0}{p_0}$, represents the amount of degradation, p represents the IC peak values and p_0 is the initial peak value. $\theta_{0\sim3}$ are the identification parameters in this equation. K_3 is not included in this equation as it is insensitive to the variation of IC peak values.

Given a set of n data points, p_i, α_{1i}, K_{1i}, α_{3i}, $i = 1, ..., n$, from one battery cell at different aging stages, the values of $\theta_{0\sim3}$ can be easily calculated from the least squares method,

$$\begin{aligned} &\theta = (\Phi^T\Phi)^{-1}\Phi^T q, \\ &\text{where} \\ &\theta = [\theta_0, \theta_1, \theta_2, \theta_3], \\ &\Phi = [\phi_1, \phi_2, ..., \phi_n]^T, \\ &q = [q_1, q_2, ..., q_n]^T, \\ &\phi_i = [1, \alpha_{1i}, K_{1i}, \alpha_{3i}]^T. \end{aligned} \tag{9}$$

The identification results of (8) are very accurate as shown in Fig. 18, where the battery testing data of one single cell (denoted as cell A) at all different ages are included.

To use the model (8) identified from cell A to 7 other cells, one can use $\theta_{1\sim3}$ directly while adjusting θ_0 such that the value of q given by (8) at the initial stage is zero. Figure 19 show that the data from two other cells, as an example, can also be fitted accurately by applying $\theta_{1\sim3}$ without further identification effort. In other words, the IC peak values of different cells can be estimated/predicted based on the parameters $\theta_{1\sim3}$ identified from one reference cell. Therefore it is possible to perform battery SOH monitoring directly using (8) without numerically deriving the IC curves.

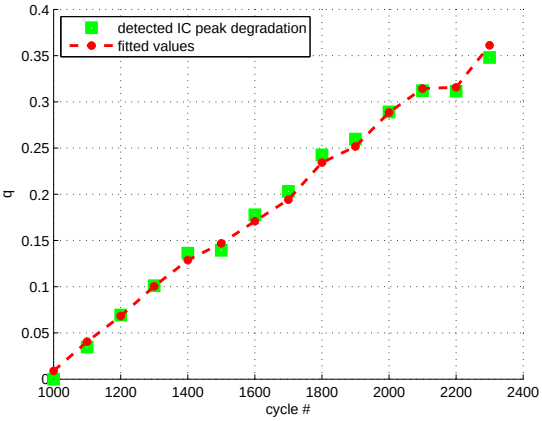

Figure 18: Identification results of (8) using battery testing data from one single cell

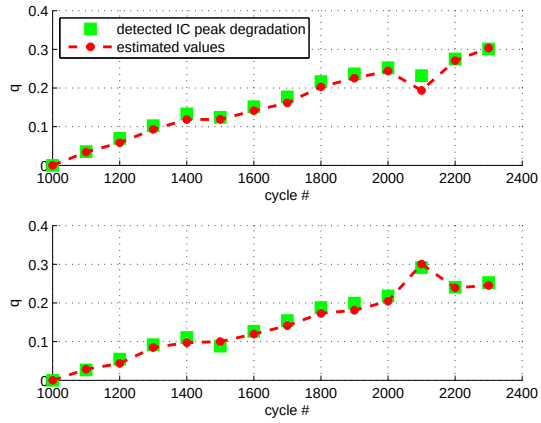

Figure 19: Verification of (8) using parameters $\theta_{1\sim3}$ identified from Fig. 18 with data from two other cells

To summarize, the simplified OCV model is capable of capturing the battery aging features with fewer parameters, thereby improving the identification efficiency and making the model implementable in on-board BMS. With the established linear relationship between the IC peak values and the OCV model parameters in (8), the battery aging information can be revealed by only looking at the parameters.

7. Conclusions

In this paper, we propose a new OCV parametric model. The special parametrization considers the staging phenomenon during the lithium intercalation/deintercalation process for lithium-ion batteries,

therefore leading to a much better fitting accuracy when applied to experimental battery OCV data. The new parametric model is applied, together with an EKF, to SOC estimation and its effectiveness is demonstrated on FUDS cycle data. We also show that the parametric model can be applied for ICA based SOH monitoring. Through comparisons of IC curves, the model is shown to be capable of reflecting battery cell's electrochemical properties at different operating temperature conditions and aging stages. Moreover, through parametric analysis, we are able to simplify the model structure and develop a function that characterizes the relations between the model parameters and the degradation of battery performance, which enables us to monitor battery SOH and estimate capacity fading only based on the model parameters. Future research will focus on developing more efficient algorithms for the determination of the OCV model parameters.

8. Acknowledgment

This work is supported by the Department of Energy under Award Number DE-PI0000012.

References

[1] M. Safari, C. Delacourt, J. Electrochem. Soc. 158 (2011) A562–A571.
[2] M. Armand, J. M. Tarascon, Nature 451 (2008) 652–657.
[3] M. A. Roscher, D. U. Sauer, J. Power Sources 196 (2011) 331–336.
[4] B. Dunn, H. Kamath, J.-M. Tarascon, Science 6058 (2011) 928–935.
[5] B. Y. Liaw, M. Dubarry, in: G. Pistoia (Ed.), Electric and Hybrid Vehicles: Power Sources, Models, Sustainability, Infrastructure and the Market, Elsevier, 2010, pp. 375–403.
[6] E. Meissner, G. Richter, J. Power Sources 116 (2003) 79–98.
[7] C. Weng, Y. Cui, J. Sun, H. Peng, J. Power Sources 235 (2013) 36–44.
[8] V. Pop, H. J. Bergveld, D. Danilov, P. P. L. Regtien, P. H. L. Notten, Battery Management Systems: Accurate State-of-Charge Indication for Battery-Powered Applications, Springer, 1st edition, 2008.
[9] S. Piller, M. Perrin, A. Jossen, J. Power Sources 96 (2001) 113–120.
[10] S. Santhanagopalan, R. E. White, J. Power Sources 161 (2006) 1346–1355.
[11] M. Verbrugge, E. Tate, J. Power Sources 126 (2004) 236–249.
[12] X. Hu, S. Li, H. Peng, F. Sun, J. Power Sources 217 (2012) 209–219.
[13] M. Safari, C. Delacourt, J. Electrochem. Soc. 158 (2011) A63–A73.
[14] J. Groot, State-of-Health Estimation of Li-ion Batteries: Cycle Life Test Methods, Master's thesis, Chalmers University of Technology, 2012.
[15] R. Yazami, P. Touzain, J. Power Sources 9 (1983) 365–371.
[16] J. R. Dahn, Phys. Rev. B44 (1991) 9170–9177.
[17] R. Yazami, Y. Reynier, J. Power Sources 153 (2006) 312–318.
[18] M. A. Roscher, J. Assfalg, O. S. Bohlen, IEEE Trans. Veh. Technol. 60 (2011) 98–103.
[19] M. Dubarry, V. Svoboda, R. Hwu, , B. Y. Liaw, Electrochem. Solid St. 9 (2006) A454–A457.
[20] M. Dubarry, B. Y. Liaw, J. Power Sources 194 (2009) 541–549.
[21] X. Hu, S. Li, H. Peng, J. Power Sources 198 (2012) 359–367.
[22] G. L. Plett, J. Power Sources 134 (2004) 262–276.
[23] Y. Hu, S. Yurkovich, Y. Guezennec, B. Yurkovich, J. Power Sources 196 (2011) 449–457.
[24] D. E. Neumann, S. Lichte, in: NDIA Ground Vehicle Systems Engineering and Technology Symposium.
[25] M. Chen, G. A. Rincón-Mora, IEEE Trans. Veh. Technol. 21 (2008) 504–511.
[26] A. Szumanowski, Y. Chang, IEEE Trans. Veh. Technol. 57 (2008) 1425–1432.
[27] G. L. Plett, J. Power Sources 134 (2004) 277–292.
[28] M. Dubarry, N. Vuillaume, B. Y. Liaw, J. Power Sources 186 (2009) 500–507.
[29] J. Vetter, P. Novák, M. Wagner, C. Veit, K.-C. Möller, J. Besenhard, M. Winter, M. Wohlfahrt-Mehrens, C. Vogler, A. Hammouched, J. Power Sources 147 (2005) 269–281.